

A Unifying Framework for Spectrum-Preserving Graph Sparsification and Coarsening

Gecia Bravo-Hermesdorf*

Princeton Neuroscience Institute
Princeton University
Princeton, NJ, 08544, USA
geciah@princeton.edu

Lee M. Gunderson*

Department of Astrophysical Sciences
Princeton University
Princeton, NJ, 08544, USA
leeg@princeton.edu

Abstract

How might one “reduce” a graph? That is, generate a smaller graph that preserves the global structure at the expense of discarding local details? There has been extensive work on both graph sparsification (removing edges) and graph coarsening (merging nodes, often by edge contraction); however, these operations are currently treated separately. Interestingly, for a planar graph, edge deletion corresponds to edge contraction in its planar dual (and more generally, for a graphical matroid and its dual). Moreover, with respect to the dynamics induced by the graph Laplacian (e.g., diffusion), deletion and contraction are physical manifestations of two reciprocal limits: edge weights of 0 and ∞ , respectively. In this work, we provide a unifying framework that captures both of these operations, allowing one to simultaneously sparsify and coarsen a graph while preserving its large-scale structure. The limit of infinite edge weight is rarely considered, as many classical notions of graph similarity diverge. However, its algebraic, geometric, and physical interpretations are reflected in the Laplacian pseudoinverse L^\dagger , which remains finite in this limit. Motivated by this insight, we provide a probabilistic algorithm that reduces graphs while preserving L^\dagger , using an unbiased procedure that minimizes its variance. We compare our algorithm with several existing sparsification and coarsening algorithms using real-world datasets, and demonstrate that it more accurately preserves the large-scale structure.

1 Motivation

Many complex structures and phenomena are naturally described as graphs (eg,¹ brains, social networks, the internet, etc). Indeed, graph-structured data are becoming increasingly relevant to the field of machine learning [2, 3, 4]. These graphs are frequently massive, easily surpassing our working memory, and often the computer’s relevant cache [5]. It is therefore essential to obtain smaller approximate graphs to allow for more efficient computation.

Graphs are defined by a set of nodes V and a set of edges $E \subseteq V \times V$ between them, and are often represented as an adjacency matrix A with size $|V| \times |V|$ and density $\propto |E|$. Reducing either of these quantities is advantageous: graph “coarsening” focuses on the former, aggregating nodes while respecting the overall structure, and graph “sparsification” on the latter, preferentially retaining the important edges.

*Both authors contributed equally to this work.

¹The authors agree with the sentiment of the footnote on page xv of [1], viz, omitting superfluous full stops to obtain a more efficient compression of, eg: *videlicet*, *exempli gratia*, etc.

Spectral graph sparsification has revolutionized the field of numerical linear algebra and is used, eg, in algorithms for solving linear systems with symmetric diagonally dominant matrices in nearly-linear time [6, 7] (in contrast to the fastest known algorithm for solving general linear systems, taking $\mathcal{O}(n^\omega)$ -time, where $\omega \approx 2.373$ is the matrix multiplication exponent [8]).

Graph coarsening appears in many computer science and machine learning applications, eg: as primitives for graph partitioning [9] and visualization algorithms² [10]; as layers in graph convolution networks [3, 11]; for dimensionality reduction and hierarchical representation of graph-structured data [12, 13]; and to speed up regularized least square problems on graphs [14], which arise in a variety of problems such as ranking [15] and distributed synchronization of clocks [16].

A variety of algorithms, with different objectives, have been proposed for both sparsification and coarsening. However, a frequently recurring theme is to consider the graph Laplacian $L = D - A$, where D is the diagonal matrix of node degrees. Indeed, it appears in a wide range of applications, eg: its spectral properties can be leveraged for graph clustering [17]; it can be used to efficiently solve min-cut/max-flow problems [18]; and for undirected, positively weighted graphs (the focus of this paper), it induces a natural quadratic form, which can be used, eg, to smoothly interpolate functions over the nodes [19].

Work on spectral graph sparsification focuses on preserving the Laplacian quadratic form $\vec{x}^\top L \vec{x}$, a popular measure of spectral similarity suggested by Spielman & Teng [6]. A key result in this field is that any dense graph can be sparsified to $\mathcal{O}(|V| \log |V|)$ edges in nearly linear time using a simple probabilistic algorithm [20]: start with an empty graph, include edges from the original graph with probability proportional to their effective resistance, and appropriately reweight those edges so as to preserve $\vec{x}^\top L \vec{x}$ within a reasonable factor.

In contrast to the firm theoretical footing of spectral sparsification, work on graph coarsening has not reached a similar maturity; while a variety of spectral coarsening schemes have been recently proposed, algorithms frequently rely on heuristics, and there is arguably no consensus. Eg: Jin & Jaja [21] use k eigenvectors of the Laplacian as feature vectors to perform k -means clustering of the nodes; Purohit et al. [22] aim to minimize the change in the largest eigenvalue of the adjacency matrix; and Loukas & Vnderghelynst [23] focuses on a “restricted” Laplacian quadratic form.

Although recent work has combined sparsification and coarsening [24], they used separate algorithmic primitives, essentially analyzing the serial composition of the above algorithms. The primary contribution of this work is to provide a unifying probabilistic framework that allows one to simultaneously sparsify and coarsen a graph while preserving its global structure by using a *single* cost function that preserves the Laplacian pseudoinverse L^\dagger .

Corollary contributions include: **1)** Identifying the limit of infinite edge weight with edge contraction, highlighting how its algebraic, geometric, and physical interpretations are reflected in L^\dagger , which remains finite in this limit (Section 2); **2)** Offering a way to quantitatively compare the effects of edge deletion and edge contraction (Section 2 and 3); **3)** Providing a probabilistic algorithm that reduces graphs while preserving L^\dagger , using an unbiased procedure that minimizes its variance (Sections 3 and 4); **4)** Proposing a more sensitive measure of spectral similarity of graphs, inspired by the Poincaré half-plane model of hyperbolic space (Section 5.3); and **5)** Comparing our algorithm with several existing sparsification and coarsening algorithms using synthetic and real-world datasets, demonstrating that it more accurately preserves the large-scale structure (Section 5).

2 Why the Laplacian pseudoinverse

Many computations over graphs involve solving $L\vec{x} = \vec{b}$ for \vec{x} [25]. Thus, the algebraically relevant operator is arguably the Laplacian pseudoinverse L^\dagger . In fact, its connection with random walks has been used to derive useful measures of distances on graphs, such as the well-known effective resistance [26], and the recently proposed resistance perturbation distance [27]. Moreover, taking the pseudoinverse of L leaves its eigenvectors unchanged, but inverts the nontrivial eigenvalues. Thus, as the largest eigenpairs of L^\dagger are associated with global structure, preserving its action will preferentially maintain the overall “shape” of the graph (see Appendix Section G for details). For instance, the Fielder vector [17] (associated with the “algebraic connectivity” of a graph) will be

²For animated examples using our graph reduction algorithm, see the following link:
youtube.com/playlist?list=PLmfiQcz2q6d3sZutLri4ZAIDLqM_4K1p-.

preferentially preserved. We now discuss in further detail why L^\dagger is well-suited for both graph sparsification and coarsening.

Attention is often restricted to undirected, positively weighted graphs [28]. These graphs have many convenient properties, eg, their Laplacians are positive semidefinite ($\vec{x}^\top L \vec{x} \geq 0$) and have a well-understood kernel and cokernel ($L\vec{1} = \vec{1}^\top L = \vec{0}$). The edge weights are defined as a mapping $W: E \rightarrow \mathbb{R}_{>0}$. When the weights represent connection strength, it is generally understood that $w_e \rightarrow 0$ is equivalent to removing edge e . However, the closure of the positive reals has a reciprocal limit, namely $w_e \rightarrow +\infty$.

This limit is rarely considered, as many classical notions of graph similarity diverge. This includes the standard notion of spectral similarity, where \tilde{G} is a σ -spectral approximation of G if it preserves the Laplacian quadratic form $\vec{x}^\top L_G \vec{x}$ to within a factor of σ for all vectors $\vec{x} \in \mathbb{R}^{|V_G|}$ [6]. Clearly, this limit yields a graph that does not approximate the original for any choice of σ : any \vec{x} with different values for the two nodes joined by the edge with infinite weight now yields an infinite quadratic form. This suggests considering only vectors that have the same value for these two nodes, essentially contracting them into a single “supernode”. Algebraically, this interpretation is reflected in L^\dagger , which remains finite in this limit: the pair of rows (and columns) corresponding to the contracted nodes become identical (see Appendix Section C).

Physically, consider the behavior of the heat equation $\partial_t \vec{x} + L \vec{x} = \vec{0}$: as $w_e \rightarrow +\infty$, the values on the two nodes immediately equilibrate between themselves, and remain tethered for the rest of the evolution.³ Geometrically, the reciprocal limits of $w_e \rightarrow 0$ and $w_e \rightarrow +\infty$ have dual interpretations: consider a planar graph and its planar dual; edge deletion in one graph corresponds to contraction in the other, and vice versa. This naturally extends to nonplanar graphs via their graphical matroids and their duals [29].

Finally, while the Laplacian operator is frequently considered in the graph sparsification and coarsening literature, its pseudoinverse also has many important applications in the field of machine learning [30], eg: online learning over graphs [31]; similarity prediction of network data [32]; determining important nodes [33]; providing a measure of network robustness to multiple failures [34]; extending principal component analysis to graphs [35]; and collaborative recommendation systems [36]. Hence, graph reduction algorithms that preserve L^\dagger would be useful to the machine learning community.

3 Our graph reduction framework

We now describe our framework for constructing probabilistic algorithms that generate a reduced graph \tilde{G} from an initial graph G , motivated by the following desiderata: **1)** Reduce the number of edges/nodes (Section 3.1); **2)** Preserve L^\dagger in expectation (Section 3.2); and **3)** Minimize the change in L^\dagger (Section 3.3).

We first define these goals more formally. Then, in Section 3.4, we combine these requirements to define our cost function and derive the optimal probabilistic action (ie, deletion, contraction, or reweight) to perform to an edge.

3.1 Reducing edges and nodes

Depending on the application, it might be more important to reduce the number of nodes (eg, coarsening a sparse network) or the number of edges (eg, sparsifying a dense network). Let r be the number of prioritized items reduced during a particular iteration. When those items are nodes, then $r = 0$ for a deletion, and $r = 1$ for a contraction. When those items are edges, then $r = 1$ for a deletion, however $r > 1$ for a contraction is possible: if the contracted edge forms a triangle in the original graph, then the other two edges will become parallel in the reduced graph (see Figure SI 3 in Appendix Section C). With respect to the Laplacian, this is equivalent to a single edge with weight given by the sum of these now parallel edges. Thus, when edge reduction is prioritized, a contraction will have $r = 1 + \tau_e$, where τ_e is the number of triangles in the original graph G in which the contracted edge e participates.

³In the spirit of another common analogy (edge weights as conductances of a network of resistors), breaking a resistor is equivalent to deleting that edge, while contraction amounts to completely soldering over it.

Note that, even when node reduction is prioritized, the number of edges will also necessarily decrease. Conversely, when edge reduction is prioritized, contraction of an edge is also possible, thereby reducing the number of nodes as well. For the case of simultaneously sparsifying *and* coarsening a graph, we choose to prioritize edge reduction, although nodes could also be a sensible choice.

3.2 Preserving the Laplacian pseudoinverse

Consider perturbing the weight of a single edge $e = (v_1, v_2)$ by Δw . The change in the Laplacian is

$$\mathbf{L}_{\bar{G}} - \mathbf{L}_G = \Delta w \vec{b}_e \vec{b}_e^\top, \quad (1)$$

where $\mathbf{L}_{\bar{G}}$ and \mathbf{L}_G are the perturbed and original Laplacians, respectively, and \vec{b}_e is the (arbitrarily) signed incidence (column) vector associated with edge e , with entries

$$(b_e)_i = \begin{cases} +1 & i = v_1 \\ -1 & i = v_2 \\ 0 & \text{otherwise.} \end{cases} \quad (2)$$

The change in \mathbf{L}^\dagger is given by the Woodbury matrix identity⁴ [39]:

$$\mathbf{L}_{\bar{G}}^\dagger - \mathbf{L}_G^\dagger = -\frac{\Delta w}{1 + \Delta w \vec{b}_e^\top \mathbf{L}_G^\dagger \vec{b}_e} \mathbf{L}_G^\dagger \vec{b}_e \vec{b}_e^\top \mathbf{L}_G^\dagger. \quad (3)$$

Note that this change can be expressed as a matrix that depends *only* on the choice of edge e , multiplied by a scalar term that depends (nonlinearly) on the change to its weight:

$$\Delta \mathbf{L}^\dagger = \underbrace{f\left(\frac{\Delta w}{w_e}, w_e \Omega_e\right)}_{\text{nonlinear scalar}} \times \underbrace{\mathbf{M}_e}_{\text{constant matrix}}, \quad (4)$$

where

$$f = -\frac{\frac{\Delta w}{w_e}}{1 + \frac{\Delta w}{w_e} w_e \Omega_e}, \quad (5)$$

$$\mathbf{M}_e = w_e \mathbf{L}_G^\dagger \vec{b}_e \vec{b}_e^\top \mathbf{L}_G^\dagger, \quad (6)$$

$$\Omega_e = \vec{b}_e^\top \mathbf{L}_G^\dagger \vec{b}_e. \quad (7)$$

Hence, if the probabilistic reweight of this edge is chosen such that $\mathbb{E}[f] = 0$, then we have $\mathbb{E}[\mathbf{L}_{\bar{G}}^\dagger] = \mathbf{L}_G^\dagger$, as desired. Importantly, f remains finite in the following relevant limits:

$$\begin{array}{ll} \text{deletion:} & \frac{\Delta w}{w_e} \rightarrow -1, \quad f \rightarrow (1 - w_e \Omega_e)^{-1} \\ \text{contraction:} & \frac{\Delta w}{w_e} \rightarrow +\infty, \quad f \rightarrow -(w_e \Omega_e)^{-1}. \end{array} \quad (8)$$

Note that f diverges when considering deletion of an edge with $w_e \Omega_e = 1$ (ie, an edge cut). Indeed, such an action would disconnect the graph and invalidate the use of equation (3) (see footnote 4). However, this possibility is precluded by the requirement that $\mathbb{E}[f] = 0$.

3.3 Minimizing the error

Minimizing the magnitude of $\Delta \mathbf{L}^\dagger$ requires a choice of matrix norm, which we take to be the sum of the squares of its entries (ie, the square of the Frobenius norm). Our motivation is twofold. First, the algebraically convenient fact that the Frobenius norm of a rank one matrix has a simple form, viz,

$$m_e \equiv \|\mathbf{M}_e\|_F = w_e \vec{b}_e^\top \mathbf{L}_G^\dagger \mathbf{L}_G^\dagger \vec{b}_e. \quad (9)$$

Second, the square of this norm behaves as a variance; to the extent that the \mathbf{M}_e associated to different edges can be treated as (entrywise) uncorrelated one can decompose multiple perturbations as follows:

$$\mathbb{E}\left[\left\|\sum \Delta \mathbf{L}^\dagger\right\|_F^2\right] \approx \sum \mathbb{E}\left[\|\Delta \mathbf{L}^\dagger\|_F^2\right], \quad (10)$$

⁴This expression is only officially applicable when the initial and final matrices are full-rank; additional care must be taken when they are not. However, for the case of changing the edge weights of a graph Laplacian, the original formula remains unchanged [37, 38] (so long as the graph remains connected), provided one uses the definitions in Section 3.5 (see also Appendix Sections C and F).

which allows the single-edge results from Section 3.4 to be iteratively applied to our reduction algorithm, which has multiple reductions (Section 4). In Appendix Section A, we empirically validate this approximation using synthetic and real-world networks, showing that this approximation is either nearly exact or a conservative estimate.

For subtleties associated with edge contraction (see Appendix Section F, in particular equation (39)).

3.4 A cost function for spectral graph reduction

Combining the discussed desiderata, we choose to minimize the following cost function:

$$\mathcal{C} = \mathbb{E} \left[\left\| \Delta \mathbf{L}^\dagger \right\|_F^2 \right] - \beta^2 \mathbb{E}[r], \quad (11)$$

subject to

$$\mathbb{E}[\Delta \mathbf{L}^\dagger] = \mathbf{0}, \quad (12)$$

where the parameter β controls the tradeoff between number of prioritized items reduced r and error incurred in \mathbf{L}^\dagger . This cost function naturally arises when minimizing the expected squared error for a given expected amount of reduction (or equivalently maximizing the expected number of reductions for a given expected squared error).

We desire to minimize this cost function over all possible reduced graphs. As, when reducing multiple edges, $\mathbb{E}[r]$ is additive and the expected squared error is empirically additive, we are able to decompose this objective into a sequence of minimizations applied to individual edges. Thus, minimization of this cost function for each edge acted upon can be seen as a probabilistic greedy algorithm for minimizing the cost function for the final reduced graph.

Here, we describe the analytic solution for the optimal action (ie, probabilistically choosing to delete, contract, or reweight) to be applied to a single edge. We provide the solution in Figure 1, and a detailed derivation in Appendix Section B.

For a given edge e , the values of m_e , $w_e \Omega_e$, and τ_e are fixed, and minimizing the cost function (11) (given (12)) results in a piecewise solution with three regimes, depending on the value of β : **1)** When $\beta < \beta_1(m_e, w_e \Omega_e, \tau_e) = \min(\beta_{1d}, \beta_{1c})$, β is small compared with the error that would be incurred by acting on this edge, thus it should not be changed; **2)** When $\beta > \beta_2(m_e, w_e \Omega_e, \tau_e)$, β is large for this edge, and the optimal solution is to probabilistically delete or contract this edge ($p_d + p_c = 1$; no reweight is required); and **3)** In the intermediate case ($\beta_1 < \beta < \beta_2$), there are two possibilities, depending on the edge and the choice of prioritized items: if $\beta_{1d} < \beta_{1c}$, the edge is either deleted or reweighted, and if $\beta_{1c} < \beta_{1d}$, the edge is either contracted or reweighted.

$\beta < \beta_1$	$p_d = 0, \quad p_c = 0, \quad \frac{\Delta w}{w_e} = 0$		prioritizing edges	prioritizing nodes	
$\beta_1 < \beta < \beta_2$	$\beta_{1d} < \beta_{1c}$	$p_d = 1 - \frac{m_e}{(1 - w_e \Omega_e) \beta}, \quad p_c = 0,$ $\frac{\Delta w}{w_e} = \left(1 - \frac{p_d}{1 - w_e \Omega_e}\right)^{-1} - 1$	β_{1d}	$\frac{m_e}{1 - w_e \Omega_e}$	∞
	$\beta_{1c} < \beta_{1d}$	$p_d = 0, \quad p_c = 1 - \frac{m_e}{w_e \Omega_e \beta \sqrt{1 + \tau_e}},$ $\frac{\Delta w}{w_e} = -\frac{p_c}{w_e \Omega_e}$	β_{1c}	$\frac{m_e}{w_e \Omega_e} \frac{1}{\sqrt{1 + \tau_e}}$	$\frac{m_e}{w_e \Omega_e}$
$\beta > \beta_2$	$p_d = 1 - w_e \Omega_e, \quad p_c = w_e \Omega_e$	β_2	$\frac{m_e}{w_e \Omega_e (1 - w_e \Omega_e)} \frac{1}{1 + \sqrt{1 + \tau_e}}$	$\frac{m_e}{w_e \Omega_e (1 - w_e \Omega_e)}$	

Figure 1: *Left: Minimizing \mathcal{C} for a single edge e .* There are three regimes for the solution, depending on the value of β . When node reduction is prioritized, set $\tau_e = 0$. *Right: Values of β dividing the three regimes.* Note that when edge reduction is prioritized, the number of triangles enters the expressions, and when node reduction is prioritized, there is no deletion in the intermediate regime. However, for either choice, both deletion and contraction can have finite probability, and the algorithm does not exclusively reduce one or the other. Thus, when simultaneously sparsifying and coarsening a graph, the prioritized items may be chosen to be either edges or nodes. We remark that the values of β_{1d} , β_{1c} , and β_2 might be of independent interest as measures of edge importance for analyzing connections in real-world networks.

3.5 Node-weighted Laplacian

When nodes are merged, one often represents the connectivity of the resulting graph \tilde{G} by a matrix of smaller size. To properly compare the spectral properties of \tilde{G} with those of the original graph G , one must keep track of the number of original nodes that comprise these “supernodes” and assign them proportional weights. The appropriate reduced Laplacian $\mathbf{L}_{\tilde{G}}$ (of size $|V_{\tilde{G}}| \times |V_{\tilde{G}}|$) is then $\mathbf{W}_n^{-1} \mathbf{B}^\top \mathbf{W}_e \mathbf{B}$, where the \mathbf{W} are the diagonal matrices of the node weights⁵ and the edge weights of \tilde{G} , respectively, and \mathbf{B} is its signed incidence matrix with columns given by (2).

Moreover, one must be careful to choose the appropriate pseudoinverse of $\mathbf{L}_{\tilde{G}}$, which is given by

$$\mathbf{L}_{\tilde{G}}^\dagger = (\mathbf{L}_{\tilde{G}} + \mathbf{J})^{-1} - \mathbf{J}, \quad (13)$$

$$\mathbf{J} = \frac{1}{\mathbf{1}^\top \vec{w}_n} \mathbf{1} \vec{w}_n^\top, \quad (14)$$

where $\vec{w}_n \in \mathbb{R}_{>0}^{|V_{\tilde{G}}|}$ is the vector of node weights. Note that $\mathbf{L}_{\tilde{G}}^\dagger \mathbf{L}_{\tilde{G}} = \mathbf{L}_{\tilde{G}} \mathbf{L}_{\tilde{G}}^\dagger = \mathbf{I} - \mathbf{J}$, the appropriate node-weighted projection matrix.

To compare the action of the original and reduced Laplacians on a vector $\vec{x} \in \mathbb{R}^{|V_{\tilde{G}}|}$ over the nodes of the original graph, one must “lift” $\mathbf{L}_{\tilde{G}}$ to operate on the same space as \mathbf{L}_G . We thus define the mapping from original to coarsened nodes as a $|V_{\tilde{G}}| \times |V_G|$ matrix \mathbf{C} , with entries

$$c_{ij} = \begin{cases} 1 & \text{node } j \text{ in supernode } i \\ 0 & \text{otherwise.} \end{cases} \quad (15)$$

The appropriate lifted Laplacian is $\mathbf{L}_{G,l} = \mathbf{C}^\top \mathbf{L}_{\tilde{G}} \mathbf{W}_n^{-1} \mathbf{C}$. Likewise, the lifted Laplacian pseudoinverse is $\mathbf{L}_{G,l}^\dagger = \mathbf{C}^\top \mathbf{L}_{\tilde{G}}^\dagger \mathbf{W}_n^{-1} \mathbf{C}$ (see Appendix Section C for a detailed rationale of these definitions).

4 Our graph reduction algorithm

Using this framework, we now describe our graph reduction algorithm. Similar to many graph coarsening methods [41, 42], we obtain the reduced graph by acting on the initial graph (as opposed to adding edges to an empty graph, as is frequently done in sparsification [43, 44]).

Care must be taken, however, as simultaneous deletions/contractions may result in undesirable behavior. Eg, while any edge that is itself a cut-set will never be deleted (as $w_e \Omega_e = 1$), a collection of edges that together make a cut-set might all have finite deletion probability. Hence, if multiple edges are simultaneously deleted, the graph could become disconnected. In addition, the single-edge analysis could underestimate the change in \mathbf{L}^\dagger associated with simultaneous contractions. Eg, consider two highly-connected nodes that are each the center of a different community, and a third auxiliary node that happens to be connected to both: contracting the auxiliary node into either of the other two would be sensible, but performing both contractions would merge the two communities.

Algorithm 1 describes our graph reduction scheme. Its inputs are: G , the original graph; q , the fraction of sampled edges to act upon per iteration; d , the minimum expected decrease in prioritized items per edge acted upon; and `StopCriterion`, a user-defined function. With these inputs, we implicitly select β . Let $\beta_{*,e}$ be the minimum β such that $\mathbb{E}[r] \geq d$ for edge e . For each iteration, we compute $\beta_{*,e}$ for all sampled edges, and choose a β such that a fraction q of them have $\beta_{*,e} < \beta$. We then apply the corresponding probabilistic actions to these edges. The appropriate choice of `StopCriterion` depends on the application. Eg, if one desires to bound the accuracy of an algorithm that uses graph reduction as a primitive, limiting the Frobenius error in \mathbf{L}^\dagger is a sensible choice (it is trivial to keep a running total of the estimated error, see Appendix Section A). On the other hand, if one would like the reduced graph to be no larger than a certain size, then one can simply continue reducing until this point. While both criteria may also be implicitly implemented via an upper bound on β , the relationship is nontrivial and depends on the structure of the graph.

The aforementioned problems associated with simultaneous deletions/contractions can be eliminated by taking a conservative approach: acting on only a single edge per iteration. However, this results in an algorithm that does not scale favorably for large graphs. A more scalable solution involves

⁵ \mathbf{W}_n is often referred to as the “mass matrix” [40]. We note that the use of the random walk matrix $\mathbf{D}^{-1} \mathbf{L}$ can be seen as using the node degrees as a surrogate for the node weights.

Algorithm 1 ReduceGraph

```
1: Inputs: graph  $G$ , fraction of sampled edges to act upon  $q$ , minimum  $\mathbb{E}[r]$  per edge acted upon  $d$ , and a
   StopCriterion
2: Initialize  $\tilde{G}_0 \leftarrow G$ ,  $t \leftarrow 0$ ,  $stop \leftarrow \text{False}$ 
3: while not ( $stop$ ) do
4:   Sample an independent edge set
5:   for (edge  $e$ ) in (sampled edges) do
6:     Compute  $\Omega_e, m_e$  (see equations (7) and (9))
7:     Evaluate  $\beta_{*e}$ , according to  $d$  (see Tables in Figure 1)
8:   end for
9:   Choose  $\beta$  such that a fraction  $q$  of the sampled edges (those with the lowest  $\beta_{*e}$ ) are acted upon
10:  Probabilistically choose to reweight, delete, or contract these edges
11:  Perform reweights and deletions to  $\tilde{G}_t$ 
12:  Perform contractions to  $\tilde{G}_t$ 
13:   $\tilde{G}_{t+1} \leftarrow \tilde{G}_t$ ,  $t \leftarrow t + 1$ 
14:   $stop \leftarrow \text{StopCriterion}(\tilde{G}_t)$ 
15: end while
16: return reduced graph  $\tilde{G}_t$ 
```

carefully sampling the candidate set of edges. In particular, we are able to significantly ameliorate these issues by sampling the candidate edges such that they do not have any nodes in common (ie, the sampled edges form an independent edge set). Not only does this eliminate the possibility of “accidental” contractions, but, empirically, it also suppresses the occurrence of graph disconnections (the small fraction that become disconnected are restarted). At each iteration, our algorithm finds a random maximal independent edge set in $\mathcal{O}(|V|)$ time using a simple greedy algorithm.⁶ In practice, the size of such a set scales as $\mathcal{O}(|V|)$ (although it is easy to find families for which this scaling does not hold, eg, star graphs). Our algorithm then computes the Ω_e and m_e of these sampled edges, and acts on the fraction q with the lowest β_{*e} .

The main computational bottleneck of our algorithm is computing Ω_e and m_e (equation (9)). However, we can draw on the work of [20], which describes a method for efficiently computing ε -approximate values of Ω_e for all edges, requiring $\tilde{\mathcal{O}}(|E| \log |V| / \varepsilon^2)$ time. With minimal changes, this procedure can also be used to compute approximate values of m_e with similar efficiency (in Appendix Section F, we discuss the details of how to efficiently compute approximations of m_e). As we must compute these quantities for each iteration, we multiply the running time by the expected number of iterations, $\mathcal{O}(|E|/qd|V|)$. Empirically, we find that one is able to set $q \sim 1/16$ and $d \sim 1/4$ with minimal loss in reduction quality (see Appendix Section E). Thus, we expect that our algorithm could have a running time of $\tilde{\mathcal{O}}(\langle k \rangle |E|)$, where $\langle k \rangle$ is the average degree. However, in the following results, we have used a naive implementation: computing L^\dagger at the onset, and updating it using the Woodbury matrix identity.

5 Experimental results

In this section, we empirically validate our framework and compare it with existing algorithms. We consider two cases of our general framework, namely graph sparsification (excluding regimes involving edge contraction), and graph coarsening (prioritizing reduction of nodes). In addition, as graph reduction is often used in graph visualization, we generated videos of our algorithm simultaneously sparsifying and coarsening several real-world datasets (see footnote 2 and Appendix Section I).

5.1 Hyperbolic interlude

When comparing a graph G with its reduced approximation \tilde{G} , it is natural to consider how relevant linear operators treat the same input vector. If the vector $L_{\tilde{G},t}\vec{x}$ is aligned with $L_G\vec{x}$, the fractional error in the quadratic form $\vec{x}^\top L \vec{x}$ is a natural quantity to consider, as it corresponds to the relative change in the magnitude of these vectors. However, it is not so clear how to compare output vectors that have

⁶Specifically, randomly permute the nodes, and sequentially pair them with a random available neighbor (if there is one). The obtained set contains at least half as many edges as the maximum matching [45].

an angular difference. Here, we describe a natural extension of this notion of fractional error, which draws intuition from the Poincaré half-plane model of hyperbolic geometry. In particular, we choose the boundary of the half-plane to be perpendicular to \vec{x} and compute the geodesic distance between $\mathbf{L}_G \vec{x}$ and $\mathbf{L}_{\tilde{G},l} \vec{x}$, viz,

$$d_{\vec{x}}(\mathbf{L}_0, \mathbf{L}_1) \stackrel{\text{def}}{=} \text{arccosh} \left(1 + \frac{\|(\mathbf{L}_0 - \mathbf{L}_1)\vec{x}\|_2^2 \|\vec{x}\|_2^2}{2(\vec{x}^\top \mathbf{L}_0 \vec{x})(\vec{x}^\top \mathbf{L}_1 \vec{x})} \right), \quad (16)$$

where \mathbf{L}_0 and \mathbf{L}_1 are positive definite matrices (for now).

We define the hyperbolic distance between these matrices as

$$d_h(\mathbf{L}_0, \mathbf{L}_1) \stackrel{\text{def}}{=} \sup_{\vec{x}} d_{\vec{x}}(\mathbf{L}_0, \mathbf{L}_1). \quad (17)$$

This dimensionless quantity inherits the following standard desirable features of a distance: symmetry and non-negativity, $d_h(\mathbf{L}_0, \mathbf{L}_1) = d_h(\mathbf{L}_1, \mathbf{L}_0) \geq 0$; identity of indiscernibles, $d_h(\mathbf{L}_0, \mathbf{L}_1) = 0 \iff \mathbf{L}_0 = \mathbf{L}_1$; and subadditivity, $d_h(\mathbf{L}_0, \mathbf{L}_2) \leq d_h(\mathbf{L}_0, \mathbf{L}_1) + d_h(\mathbf{L}_1, \mathbf{L}_2)$. In addition, we note that $d_h(c\mathbf{L}_0, c\mathbf{L}_1) = d_h(\mathbf{L}_0, \mathbf{L}_1) \forall c \in \mathbb{R} \setminus \{0\}$, emphasizing its interpretation as a fractional error.

This notion naturally extends to (positive semidefinite) graph Laplacians if one considers only vectors \vec{x} that are orthogonal to their kernels (ie, require that $\mathbf{1}^\top \vec{x} = 0$ when taking the supremum in (17)). With this modification, the connection with the spectral graph sparsification can be stated as follows:

Theorem 1. *If $d_h(\mathbf{L}_G, \mathbf{L}_{\tilde{G}}) \leq \ln(\sigma)$, then \tilde{G} is a σ -spectral approximation of G .*

Here, the notion of σ -spectral approximation is the same as in Spielman & Teng [6] (see Section 2), and thus is restricted to sparsification only. The proof is provided in Appendix Section D.

As $d_{\vec{x}}$ is analogous to the ratio of quadratic forms with \vec{x} , d_h is likewise analogous to the notion of a σ -spectral approximation. Moreover, as $d_{\vec{x}}$ and d_h also consider angular differences between $\mathbf{L}_G \vec{x}$ and $\mathbf{L}_{\tilde{G},l} \vec{x}$, they serve as more sensitive measures of graph similarity.

In the following sections, we compare our algorithm with other graph reduction methods using $d_{\vec{x}}$, where we choose \vec{x} to be eigenvectors of the original graph Laplacian. In Appendix Section H, we replicate our results using more standard measures (eg, quadratic forms and eigenvalues).

5.2 Comparison with spectral graph sparsification

Figure 2 compares our algorithm (prioritizing edge reduction, and excluding the possibility of contraction) with the standard spectral sparsification algorithm of Spielman & Srivastava [20] using three real-world datasets. We choose to compare with this particular sparsification method because it directly aims to optimally preserve the Laplacian. To the best of our knowledge, other sparsification methods either do not explicitly preserve properties associated with the Laplacian [46, 47], or share the same spirit as Spielman & Srivastava’s algorithm [48] (often considering other settings, such as distributed [49] or streaming [50] computation). The results in Figure 2 show that our algorithm better preserves \mathbf{L}^\dagger and preferentially preserves its action on eigenvectors associated with global structure.

5.3 Comparison with graph coarsening algorithms

Figure 3 compares our algorithm (prioritizing node reduction) with several existing coarsening algorithms using three more real-world datasets. In order to make a fair comparison with these existing methods, after contracting their prescribed groups of nodes, we appropriately lift the resulting reduced $\mathbf{L}_{\tilde{G}}^\dagger$ (see Appendix Section C). We find that our algorithm more accurately preserves global structure.

6 Conclusion

In this work, we unify spectral graph sparsification and coarsening through the use of a single cost function that preserves the Laplacian pseudoinverse \mathbf{L}^\dagger . We describe a probabilistic algorithm for

graph reduction that employs edge deletion, contraction, and reweighting to keep $\mathbb{E}[\mathbf{L}_G^\dagger] = \mathbf{L}_G^\dagger$, and uses a new measure of edge importance (β_*) to minimize its variance. Using synthetic and real-world datasets, we demonstrate that our algorithm more accurately preserves global structure compared to existing algorithms. We hope that our framework (or some perturbation of it) will serve as a useful tool for graph algorithms, numerical linear algebra, and machine learning.

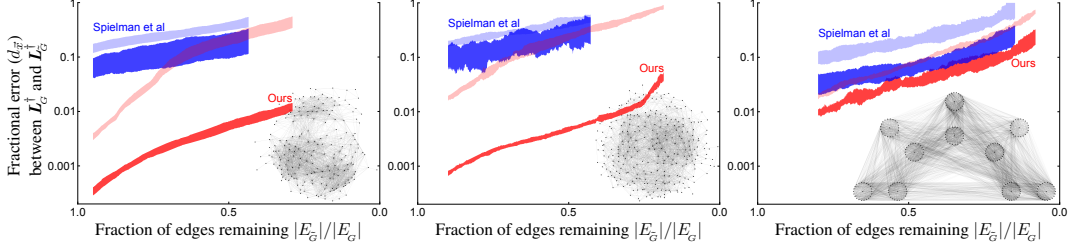


Figure 2: **Our sparsification algorithm preferentially preserves global structure.** We applied our algorithm without contraction (**Ours**) and compare with that of Spielman & Srivastava [20] (**Spielman et al**) using three datasets: *Left*: a collaboration network of Jazz musicians (198 nodes and 2742 edges) from [51]; *Middle*: the *C. elegans* posterior nervous system connectome (269 nodes and 2902 edges) from [52]; and *Right*: a weighted social network of face-to-face interactions between primary school students, with initial edge weights proportional to the number of interactions between pairs of students (236 nodes and 5899 edges) from [53]. For the two algorithms, we compute the hyperbolic distance $d_{\vec{x}}$ (fractional error) between $\mathbf{L}_G^\dagger \vec{x}$ and $\mathbf{L}_G^\dagger \vec{x}$ at different levels of sparsification for two choices of \vec{x} : the smallest non-trivial eigenvector of the original Laplacian (*dark shading*), which is associated with global structure; and the median eigenvector (*light shading*). Shading denotes one standard deviation about the mean for 16 runs of the algorithms. The curves end at the minimum edge density for which the sparsified graph is connected.

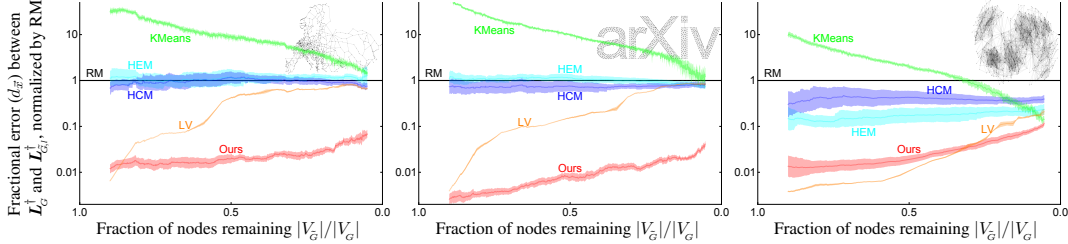


Figure 3: **Our algorithm preserves global structure more accurately than other coarsening algorithms.** We compare our algorithm (prioritizing node reduction) (**Ours**) to several existing coarsening algorithms: two classical methods for graph coarsening (heavy-edge matching (**HEM**) [54] and heavy-clique matching (**HCM**) [54]), and two recently proposed spectral coarsening algorithms (local variation by Loukas [55] (**LV**) and the *k*-means method by Jin & Jaja [21] (**KMeans**)). We ran the comparisons using three datasets: *Left*: a transportation network of European cities and roads between them (1039 nodes and 1305 edges) from [56]; *Middle*: a triangular mesh of the text “arXiv” (902 nodes and 2203 edges); and *Right*: a weighted social network of face-to-face interactions during an exhibition on infectious diseases, with initial edge weights proportional to the number of interactions between pairs of people (410 nodes and 2765 edges) from [57]. For all algorithms considered, we compute the hyperbolic distance $d_{\vec{x}}$ (fractional error) between $\mathbf{L}_G^\dagger \vec{x}$ and $\mathbf{L}_G^\dagger \vec{x}$, where \vec{x} is the smallest non-trivial eigenvector of the original Laplacian (associated with global structure). To provide a baseline, we plot their mean fractional error normalized by that obtained by random matching (**RM**) [54] for the same level of coarsening. Shading denotes one standard deviation about the mean for 16 runs of the algorithms.

Acknowledgments

We would like to thank Matthew de Courcy-Ireland for insightful discussions and Ashlyn Maria Bravo Gundermsdorff for unique perspectives.

References

- [1] Chazelle, B. *The Discrepancy Method: Randomness and Complexity* (Cambridge University Press, 2000).
- [2] Bronstein, M. M., Bruna, J., LeCun, Y., Szlam, A. & Vandergheynst, P. Geometric deep learning: Going beyond Euclidean data. *IEEE Signal Processing Magazine* **34**, 18–42 (2017).
- [3] Bruna, J., Zaremba, W., Szlam, A. & LeCun, Y. Spectral networks and locally connected networks on graphs. *International Conference on Learning Representations* (2014).
- [4] Henaff, M., Bruna, J. & LeCun, Y. Deep convolutional networks on graph-structured data. *arXiv:1506.05163* (2015).
- [5] Batson, J., Spielman, D. A., Srivastava, N. & Teng, S.-H. Spectral sparsification of graphs: Theory and algorithms. *Communications of the ACM* **56**, 87–94 (2013).
- [6] Spielman, D. A. & Teng, S.-H. Spectral sparsification of graphs. *SIAM Journal on Computing* **40**, 981–1025 (2011).
- [7] Cohen, M. B. *et al.* Solving SDD linear systems in nearly $m \log^{1/2} n$ time. *Proceedings of the 46th Annual ACM Symposium on Theory of Computing* (2014).
- [8] Le Gall, F. Powers of tensors and fast matrix multiplication. *Proceedings of the 39th International Symposium on Symbolic and Algebraic Computation* (2014).
- [9] Safo, I., Sanders, P. & Schulz, C. Advanced coarsening schemes for graph partitioning. *Journal of Experimental Algorithmics* **19**, 1.1–1.24 (2015).
- [10] Harel, D. & Koren, Y. A fast multi-scale method for drawing large graphs. *Graph Drawing* 183–196 (2001).
- [11] Simonovsky, M. & Komodakis, N. Dynamic edge-conditioned filters in convolutional neural networks on graphs. *IEEE Conference on Computer Vision and Pattern Recognition* 3693–3702 (2017).
- [12] Lafon, S. & Lee, A. Diffusion maps and coarse-graining: A unified framework for dimensionality reduction, graph partitioning, and data set parameterization. *IEEE Transactions on Pattern Analysis and Machine Intelligence* **28**, 1393–1403 (2006).
- [13] Chen, H., Perozzi, B., Hu, Y. & Skiena, S. HARP: Hierarchical representation learning for networks. *32nd AAAI Conference on Artificial Intelligence* (2018).
- [14] Hirani, A., Kalyanaraman, K. & Watts, S. Graph Laplacians and least squares on graphs. *IEEE International Parallel and Distributed Processing Symposium Workshop* 812–821 (2015).
- [15] Negahban, S., Oh, S. & Shah, D. Iterative ranking from pairwise comparisons. *Advances in Neural Information Processing Systems* 2474–2482 (2012).
- [16] Solis, R., Borkar, V. S. & Kumar, P. A new distributed time synchronization protocol for multihop wireless networks. *Proceedings of the 45th IEEE Conference on Decision and Control* 2734–2739 (2006).
- [17] Fiedler, M. Algebraic connectivity of graphs. *Czechoslovak Mathematical Journal* **23**, 298–305 (1973).
- [18] Christiano, P., Kelner, J. A., Madry, A., Spielman, D. A. & Teng, S.-H. Electrical flows, Laplacian systems, and faster approximation of maximum flow in undirected graphs. *Proceedings of the 43rd Annual ACM Symposium on Theory of Computing* 273–282 (2011).
- [19] Kyng, R., Rao, A., Sachdeva, S. & Spielman, D. A. Algorithms for Lipschitz learning on graphs. *Conference on Learning Theory* (2015).
- [20] Spielman, D. A. & Srivastava, N. Graph sparsification by effective resistances. *SIAM Journal on Computing* **40**, 1913–1926 (2011).
- [21] Jin, Y. & JaJa, J. F. Network summarization with preserved spectral properties. *arXiv:1802.04447* (2018).
- [22] Purohit, M., Prakash, B. A., Kang, C., Zhang, Y. & Subrahmanian, V. Fast influence-based coarsening for large networks. *Proceedings of the 20th ACM SIGKDD International Conference on Knowledge Discovery and Data Mining* 1296–1305 (2014).
- [23] Loukas, A. & Vandergheynst, P. Spectrally approximating large graphs with smaller graphs. *International Conference on Machine Learning* **80**, 3237–3246 (2018).

- [24] Zhao, Z., Wang, Y. & Feng, Z. Nearly-linear time spectral graph reduction for scalable graph partitioning and data visualization. *arXiv:1812.08942* (2018).
- [25] Teng, S.-H. The Laplacian paradigm: Emerging algorithms for massive graphs. *Theory and Applications of Models of Computation* 2–14 (2010).
- [26] Chandra, A. K., Raghavan, P., Ruzzo, W. L., Smolensky, R. & Tiwari, P. The electrical resistance of a graph captures its commute and cover times. *Computational Complexity* **6**, 312–340 (1996).
- [27] Monnig, N. D. & Meyer, F. G. The resistance perturbation distance: A metric for the analysis of dynamic networks. *Discrete Applied Mathematics* **236**, 347–386 (2018).
- [28] Cohen, M. B. *et al.* Almost-linear-time algorithms for Markov chains and new spectral primitives for directed graphs. *Proceedings of the 49th Annual ACM SIGACT Symposium on Theory of Computing* 410–419 (2017).
- [29] Oxley, J. G. *Matroid Theory*, vol. 3 (Oxford University Press, USA, 2006).
- [30] Ranjan, G., Zhang, Z.-L. & Boley, D. Incremental computation of pseudoinverse of Laplacian. *Lecture Notes in Computer Science* 729–749 (2014).
- [31] Herbster, M., Pontil, M. & Wainer, L. Online learning over graphs. *Proceedings of the 22nd International Conference on Machine Learning* 305–312 (2005).
- [32] Gentile, C., Herbster, M. & Pasteris, S. Online similarity prediction of networked data from known and unknown graphs. *Conference on Learning Theory* 662–695 (2013).
- [33] Van Mieghem, P., Devriendt, K. & Cetinay, H. Pseudoinverse of the Laplacian and best spreader node in a network. *Physical Review E* **96**, 032311 (2017).
- [34] Ranjan, G. & Zhang, Z.-L. Geometry of complex networks and topological centrality. *Physica A: Statistical Mechanics and its Applications* **392**, 3833–3845 (2013).
- [35] Saerens, M., Fouss, F., Yen, L. & Dupont, P. The principal components analysis of a graph, and its relationships to spectral clustering. *European Conference on Machine Learning* 371–383 (2004).
- [36] Pirotte, A., Renders, J.-M., Saerens, M. & Fouss, F. Random-walk computation of similarities between nodes of a graph with application to collaborative recommendation. *IEEE Transactions on Knowledge & Data Engineering* 355–369 (2007).
- [37] Riedel, K. S. A Sherman–Morrison–Woodbury identity for rank augmenting matrices with application to centering. *SIAM Journal on Matrix Analysis and Applications* **13**, 659–662 (1992).
- [38] Meyer, C. D., Jr. Generalized inversion of modified matrices. *SIAM Journal on Applied Mathematics* **24**, 315–323 (1973).
- [39] Woodbury, M. A. *Inverting Modified Matrices*. Memorandum Rept 42, Statistical Research Group (Princeton University, Princeton, NJ, 1950).
- [40] Koren, Y., Carmel, L. & Harel, D. ACE: A fast multiscale eigenvectors computation for drawing huge graphs. *IEEE Symposium on Information Visualization* 137–144 (2002).
- [41] Hendrickson, B. & Leland, R. W. A multilevel algorithm for partitioning graphs. *Proceedings of the 1995 ACM/IEEE Conference on Supercomputing* **95**, 1–14 (1995).
- [42] Ron, D., Safro, I. & Brandt, A. Relaxation-based coarsening and multiscale graph organization. *SIAM Journal on Multiscale Modeling & Simulation* **9**, 407–423 (2011).
- [43] Kyng, R., Pachocki, J., Peng, R. & Sachdeva, S. A framework for analyzing resparsification algorithms. *Proceedings of the 38th Annual ACM-SIAM Symposium on Discrete Algorithms* 2032–2043 (2017).
- [44] Lee, Y. T. & Sun, H. An SDP-based algorithm for linear-sized spectral sparsification. *Proceedings of the 49th Annual ACM SIGACT Symposium on Theory of Computing* 678–687 (2017).
- [45] Ausiello, G. *et al.* *Complexity and Approximation: Combinatorial Optimization Problems and their Approximability Properties* (Springer Science & Business Media, 2012).
- [46] Satuluri, V., Parthasarathy, S. & Ruan, Y. Local graph sparsification for scalable clustering. In *Proceedings of the 2011 ACM SIGMOD International Conference on Management of data*, 721–732 (ACM, 2011).
- [47] Ahn, K. J., Guha, S. & McGregor, A. Graph sketches: sparsification, spanners, and subgraphs. In *Proceedings of the 31st ACM SIGMOD-SIGACT-SIGAI symposium on Principles of Database Systems*, 5–14 (ACM, 2012).
- [48] Fung, W.-S., Hariharan, R., Harvey, N. J. & Panigrahi, D. A general framework for graph sparsification. *SIAM Journal on Computing* **48**, 1196–1223 (2019).
- [49] Koutis, I. & Xu, S. C. Simple parallel and distributed algorithms for spectral graph sparsification. *ACM Transactions on Parallel Computing (TOPC)* **3**, 14 (2016).

- [50] Kapralov, M., Lee, Y. T., Musco, C., Musco, C. P. & Sidford, A. Single pass spectral sparsification in dynamic streams. *SIAM Journal on Computing* **46**, 456–477 (2017).
- [51] Gleiser, P. M. & Danon, L. Community structure in jazz. *Advances in Complex Systems* **6**, 565–573 (2003).
- [52] Jarrell, T. A. *et al.* The connectome of a decision-making neural network. *Science* **337**, 437–444 (2012).
- [53] Stehl’e, J. *et al.* High-resolution measurements of face-to-face contact patterns in a primary school. *PloS One* **6**, e23176 (2011).
- [54] Karypis, G. & Kumar, V. A fast and high quality multilevel scheme for partitioning irregular graphs. *SIAM Journal on Scientific Computing* **20**, 359–392 (1998).
- [55] Loukas, A. Graph reduction with spectral and cut guarantees. *arXiv:1808.10650v2* (2018).
- [56] Šubelj, L. & Bajec, M. Robust network community detection using balanced propagation. *The European Physical Journal B* **81**, 353–362 (2011).
- [57] Isella, L. *et al.* What’s in a crowd? Analysis of face-to-face behavioral networks. *Journal of Theoretical Biology* **271**, 166–180 (2011).
- [58] Bell, W., Olson, L. & Schroder, J. Pyamg: Algebraic multigrid solvers in python v3. 0, 2015. URL <http://www.pyamg.org>. Release **3** (2015).

Appendix

A Empirical validation of the approximation in equation (10)

In order to derive our graph reduction algorithm, we assume that the entries of the M_e associated to different edges are approximately entrywise uncorrelated (Main Text Section 3.3). Similar to how the variance of the sum of independent random variables is the sum of their individual variances, this assumption allows us to approximate the expected squared Frobenius error of the final reduced graph $\mathbb{E}[\|\mathbf{L}_G^\dagger - \mathbf{L}_G^\dagger\|_F^2]$ as a sum over the sequence of probabilistic actions to individual edges:

$$\underbrace{\mathbb{E}\left[\left\|\sum \Delta \mathbf{L}^\dagger\right\|_F^2\right]}_{\text{true error}} \approx \underbrace{\sum \mathbb{E}\left[\left\|\Delta \mathbf{L}^\dagger\right\|_F^2\right]}_{\text{estimated error}}. \quad (18)$$

In Figure SI 1, we empirically validate this assumption for networks with a variety of structures. In fact, the true error is statistically equal to or less than the estimated error. Thus, the estimated error may be used by `StopCriterion` in Algorithm 1.

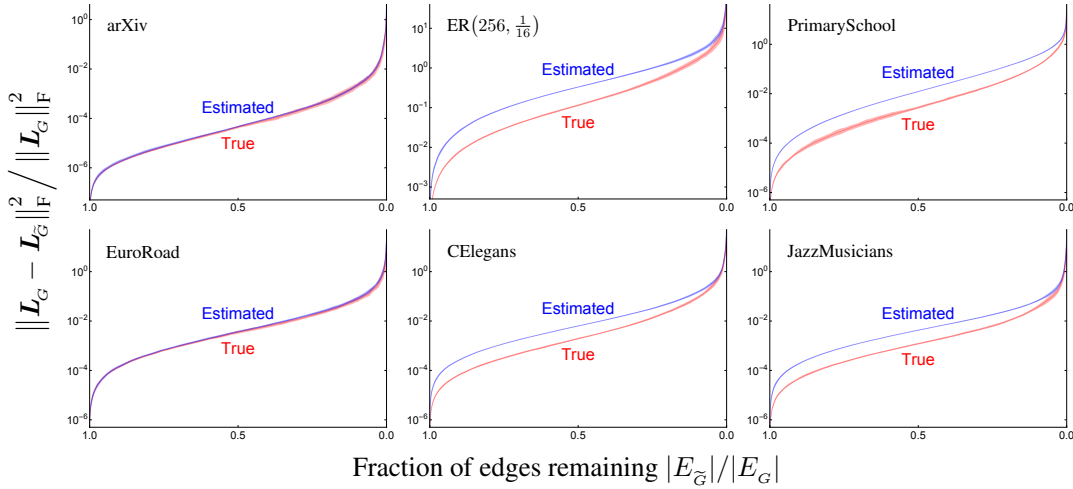


Figure SI 1: **The approximation of uncorrelated changes to \mathbf{L}^\dagger is nearly exact or a conservative estimate.** We test the validity of equation (18) using a variety of datasets: *Top left*: a triangular mesh of the text “arXiv” (902 nodes and 2203 edges); *Top middle*: an Erdős–Rényi model (256 nodes and $p = 1/16$); *Top right*: a weighted social network of face-to-face interactions between primary school students, with initial edge weights proportional to the number of interactions between pairs of students (236 nodes and 5899 edges) from [53]; *Bottom left*: a transportation network of European cities and roads between them (1039 nodes and 1305 edges) from [56]; *Bottom middle*: the *C. elegans* posterior nervous system connectome (269 nodes and 2902 edges) from [52]; and *Bottom right*: a collaboration network of Jazz musicians (198 nodes and 2742 edges) from [51]. We applied Algorithm 1, prioritizing edge reduction (allowing for deletion, contraction, and reweighting), and setting $q = 1/16$ and $d = 1/4$. We recorded the estimated error and the true error in \mathbf{L}^\dagger as a function of amount of reduction. Shading denotes one standard deviation about the mean for 32 runs of the algorithm. In general, the estimated error serves as an approximate upper bound of the true error in \mathbf{L}^\dagger (although it is nearly exact for graphs with a geometric quality). The validity of the approximation allows one to use a bound on the estimated error as a `StopCriterion` in Algorithm 1.

B Derivation of the optimal probabilistic action to an edge

As discussed in Section 3.4, we seek to minimize:

$$\mathcal{C} = \mathbb{E}\left[\left\|\Delta \mathbf{L}^\dagger\right\|_F^2\right] - \beta^2 \mathbb{E}[r], \quad (19)$$

subject to

$$\mathbb{E}[\Delta \mathbf{L}^\dagger] = \mathbf{0}. \quad (20)$$

When reducing multiple edges, $\mathbb{E}[r]$ is additive and $\mathbb{E}[\|\Delta \mathbf{L}^\dagger\|_F^2]$ is approximately additive (see Appendix Section A). Thus, we partition this minimization into a sequence of subproblems, treating each perturbation to an edge individually.

Recall that

$$\Delta \mathbf{L}^\dagger = \underbrace{f\left(\frac{\Delta w}{w_e}, w_e \Omega_e\right)}_{\text{nonlinear scalar}} \times \underbrace{\mathbf{M}_e}_{\text{constant matrix}}, \quad \text{where} \quad f = -\frac{\frac{\Delta w}{w_e}}{1 + \frac{\Delta w}{w_e} w_e \Omega_e}.$$

We now derive the optimal probability of deleting (p_d), contracting (p_c), or reweighting ($1 - p_d - p_c$) a given edge e , along with the change to its weight (Δw) in the case of the latter.

The constraint (20) requires that this reweight satisfies

$$\frac{p_d}{1 - w_e \Omega_e} - \frac{p_c}{w_e \Omega_e} + (1 - p_d - p_c) \mathbb{E}[f | \text{reweight}] = 0, \quad (21)$$

where we have used the following limits:

$$\begin{aligned} \text{deletion:} \quad & \frac{\Delta w}{w_e} \rightarrow -1, & f & \rightarrow (1 - w_e \Omega_e)^{-1} \\ \text{contraction:} \quad & \frac{\Delta w}{w_e} \rightarrow +\infty, & f & \rightarrow -(w_e \Omega_e)^{-1}. \end{aligned} \quad (22)$$

Likewise, the cost function (19) for acting on the edge e becomes:

$$\mathcal{C} = \left(\frac{p_d}{(1 - w_e \Omega_e)^2} + \frac{p_c}{(w_e \Omega_e)^2} + (1 - p_d - p_c) \mathbb{E}[f^2 | \text{reweight}] \right) m_e^2 - \beta^2 (r_d p_d + r_c p_c), \quad (23)$$

where r_d and r_c are the number of prioritized items that would be removed by a deletion or contraction, respectively.

For a fixed p_d and p_c , $\mathbb{E}[f | \text{reweight}]$ is fixed by equation (21). As $\frac{\partial^2 f}{\partial \Delta w^2} > 0$ everywhere, the inequality $\mathbb{E}[f^2 | \text{reweight}] \geq \mathbb{E}[f | \text{reweight}]^2$ becomes an equality under minimization of (23).

Thus, if an edge is to be reweighted, it will be changed by the unique Δw satisfying

$$\frac{p_d}{1 - w_e \Omega_e} - \frac{p_c}{w_e \Omega_e} - (1 - p_d - p_c) \frac{\frac{\Delta w}{w_e}}{1 + \frac{\Delta w}{w_e} w_e \Omega_e} = 0. \quad (24)$$

Clearly, the space of allowed solutions lies within the simplex \mathcal{S} : $0 \leq p_d, 0 \leq p_c, p_d + p_c \leq 1$. The additional constraint $-1 \leq \frac{\Delta w}{w_e} \leq \infty$ further implies that $p_c \leq w_e \Omega_e$ and $p_d \leq 1 - w_e \Omega_e$. Hence, we substitute (24) into (23), and minimize it over this domain (given $m_e, w_e \Omega_e, \tau_e$, and β). After some careful elementary calculus, we obtain the solution provided in Figure 1 of the Main Text.

C Lifting the matrices of a contracted graph

Here, we provide a detailed rationale for the definitions given in Section 3.5, namely, the choice of $\mathbf{L}_{\bar{G}}$ and $\mathbf{L}_{\bar{G}}^\dagger$, and how to “lift” these matrices to the original dimension $|V_G| \times |V_G|$ when edges have been contracted.

Recall the following definitions:

$$\mathbf{L}_{\bar{G}} = \mathbf{W}_n^{-1} \mathbf{B}^\top \mathbf{W}_e \mathbf{B}, \quad (25)$$

$$\mathbf{L}_{\bar{G}}^\dagger = (\mathbf{L}_{\bar{G}} + \mathbf{J})^{-1} - \mathbf{J}, \quad (26)$$

$$\mathbf{L}_{\bar{G},l} = \mathbf{C}^\top \mathbf{L}_{\bar{G}} \mathbf{W}_n^{-1} \mathbf{C}, \quad (27)$$

$$\mathbf{L}_{\bar{G},l}^\dagger = \mathbf{C}^\top \mathbf{L}_{\bar{G}}^\dagger \mathbf{W}_n^{-1} \mathbf{C}, \quad (28)$$

where

$$\mathbf{J} = \frac{1}{\mathbf{1}^\top \bar{\mathbf{w}}_n} \bar{\mathbf{1}} \bar{\mathbf{w}}_n^\top, \quad (29)$$

$$\mathbf{C} = \{c_{ij}\} = \begin{cases} 1 & \text{node } j \text{ in supernode } i \\ 0 & \text{otherwise.} \end{cases} \quad (30)$$

The above definitions ensure that the lifted $\mathbf{L}_{\bar{G},l}^\dagger$ of the contracted graph is identical to the $w_e \rightarrow \infty$ limit of the original \mathbf{L}_G^\dagger .

To illustrate the consistency of these definitions, we consider a concrete example: the line graph with 3 edges, where the center edge is to be contracted (Figure SI 2). Let the center edge have weight $w_e \gg 1$, while the other two have a fixed weight of 1.

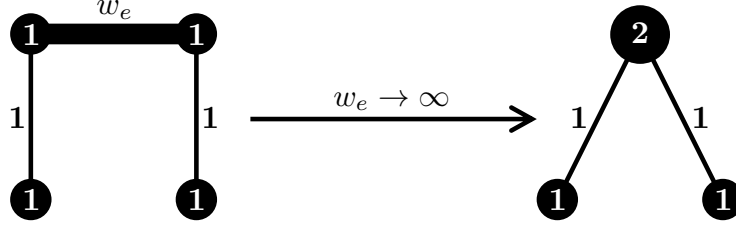


Figure SI 2: **Contracting the center edge of a line graph.** *Left:* Original graph G with large weight w_e on the center edge. *Right:* Reduced graph \tilde{G} obtained by contracting this edge ($w_e \rightarrow \infty$). Note that the weight of the contracted nodes sum to give the weight of the resulting supernode in the reduced graph.

For the original graph G , the Laplacian and its pseudoinverse are

$$\mathbf{L}_G = \begin{pmatrix} 1 & -1 & 0 & 0 \\ -1 & 1 + w_e & -w_e & 0 \\ 0 & -w_e & 1 + w_e & -1 \\ -0 & 0 & -1 & 1 \end{pmatrix}, \quad \mathbf{L}_G^\dagger = \frac{1}{8} \begin{pmatrix} 5 + \frac{2}{w_e} & -1 + \frac{2}{w_e} & -1 - \frac{2}{w_e} & -3 - \frac{2}{w_e} \\ -1 + \frac{2}{w_e} & 1 + \frac{2}{w_e} & 1 - \frac{2}{w_e} & -1 - \frac{2}{w_e} \\ -1 - \frac{2}{w_e} & 1 - \frac{2}{w_e} & 1 + \frac{2}{w_e} & -1 + \frac{2}{w_e} \\ -3 - \frac{2}{w_e} & -1 - \frac{2}{w_e} & -1 + \frac{2}{w_e} & 5 + \frac{2}{w_e} \end{pmatrix}.$$

For the contracted graph \tilde{G} , we have

$$\mathbf{W}_{\tilde{n}} = \begin{pmatrix} 1 & 0 & 0 \\ 0 & 2 & 0 \\ 0 & 0 & 1 \end{pmatrix}, \quad \mathbf{J} = \begin{pmatrix} \frac{1}{4} & \frac{1}{2} & \frac{1}{4} \\ \frac{1}{4} & \frac{1}{2} & \frac{1}{4} \\ \frac{1}{4} & \frac{1}{2} & \frac{1}{4} \end{pmatrix}, \quad \mathbf{C} = \begin{pmatrix} 1 & 0 & 0 & 0 \\ 0 & 1 & 1 & 0 \\ 0 & 0 & 0 & 1 \end{pmatrix}.$$

Thus, the reduced Laplacian and its pseudoinverse are

$$\mathbf{L}_{\tilde{G}} = \begin{pmatrix} 1 & -1 & 0 \\ -\frac{1}{2} & 1 & -\frac{1}{2} \\ 0 & -1 & 1 \end{pmatrix}, \quad \mathbf{L}_{\tilde{G}}^\dagger = \frac{1}{8} \begin{pmatrix} 5 & -2 & -3 \\ -1 & 2 & -1 \\ -3 & -2 & 5 \end{pmatrix}.$$

When lifted to the original dimensions $|V_G| \times |V_G|$, these become

$$\mathbf{L}_{\tilde{G},l} = \begin{pmatrix} 1 & -\frac{1}{2} & -\frac{1}{2} & 0 \\ -\frac{1}{2} & \frac{1}{2} & \frac{1}{2} & -\frac{1}{2} \\ -\frac{1}{2} & \frac{1}{2} & \frac{1}{2} & -\frac{1}{2} \\ 0 & -\frac{1}{2} & -\frac{1}{2} & 1 \end{pmatrix}, \quad \mathbf{L}_{\tilde{G},l}^\dagger = \frac{1}{8} \begin{pmatrix} 5 & -1 & -1 & -3 \\ -1 & 1 & 1 & -1 \\ -1 & 1 & 1 & -1 \\ -3 & -1 & -1 & 5 \end{pmatrix}.$$

Note that the lifted $\mathbf{L}_{\tilde{G},l}^\dagger$ is equal to the $w_e \rightarrow \infty$ limit of the original \mathbf{L}_G^\dagger , as desired. In contrast, the original \mathbf{L}_G diverges, while the lifted $\mathbf{L}_{\tilde{G},l}$ averages the rows and columns of the merged nodes. Moreover, regardless of whether node weights are included in the definitions, using the standard Moore–Penrose pseudoinverse of the reduced Laplacian will yield a lifted pseudoinverse that is not equivalent to the original in the $w_e \rightarrow \infty$ limit.

Additionally, we remark that, while contraction always requires the summing of node weights, it can also lead to the summing of edge weights (when the contracted edge participates in any triangle in the original graph, see Figure SI 3).

D Proof of the relationship between the hyperbolic distance and σ -spectral approximation

In this section, we prove Theorem 1 from Section 5.1:

Theorem 1. *If $d_h(\mathbf{L}_G, \mathbf{L}_{\tilde{G}}) \leq \ln(\sigma)$, then \tilde{G} is a σ -spectral approximation of G .*

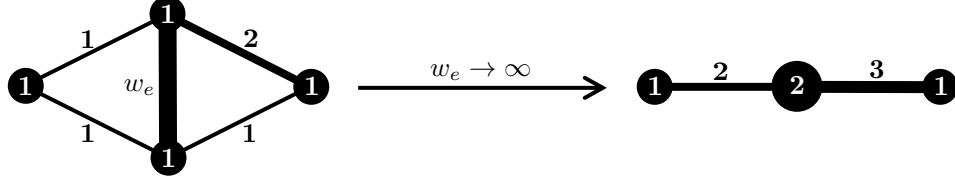


Figure SI 3: **Contracting an edge that participates in triangles.** *Left:* Original graph G containing an edge with large weight w_e that participates in two triangles. *Right:* Reduced graph \tilde{G} obtained by contracting this edge ($w_e \rightarrow \infty$). Note that the two non-contracted edges in each triangle form a single edge in the reduced graph with weight equal to their sum.

Proof. Let G be the original graph and \tilde{G} its sparse approximation (no contraction/removing of nodes). Recall the relevant definitions:

\tilde{G} is a σ -spectral approximation of G [6] if

$$\frac{1}{\sigma} \vec{x}^\top \mathbf{L}_G \vec{x} \leq \vec{x}^\top \mathbf{L}_{\tilde{G}} \vec{x} \leq \sigma \vec{x}^\top \mathbf{L}_G \vec{x}, \quad \forall \vec{x} \in \mathbb{R}^{|\mathcal{V}_G|}. \quad (31)$$

We propose to instead measure the hyperbolic distance between the resulting $\mathbf{L}_G \vec{x}$ and $\mathbf{L}_{\tilde{G}} \vec{x}$, namely

$$d_h(\mathbf{L}_G, \mathbf{L}_{\tilde{G}}) \stackrel{\text{def}}{=} \sup_{\vec{x} \perp \vec{1}} \left\{ \text{arccosh} \left(1 + \frac{\|(\mathbf{L}_G - \mathbf{L}_{\tilde{G}}) \vec{x}\|_2^2 \|\vec{x}\|_2^2}{2(\vec{x}^\top \mathbf{L}_G \vec{x})(\vec{x}^\top \mathbf{L}_{\tilde{G}} \vec{x})} \right) \right\}, \quad (32)$$

where \mathbf{L}_G and $\mathbf{L}_{\tilde{G}}$ are the Laplacians of G and \tilde{G} , respectively, and \vec{x} is perpendicular to their kernels.

Consider the result of a Laplacian acting on such a vector \vec{x} , and decompose the output as a component parallel to \vec{x} with magnitude ℓ_{\parallel} and a component $\vec{\ell}_{\perp}$ perpendicular to \vec{x} :

$$\mathbf{L}_G \vec{x} = \tilde{\ell}_{\parallel} \frac{\vec{x}}{\|\vec{x}\|_2} + \vec{\ell}_{\perp}, \quad \mathbf{L}_{\tilde{G}} \vec{x} = \tilde{\ell}_{\parallel} \frac{\vec{x}}{\|\vec{x}\|_2} + \tilde{\ell}_{\perp}. \quad (33)$$

Hence,

$$\|(\mathbf{L}_G - \mathbf{L}_{\tilde{G}}) \vec{x}\|_2^2 = (\ell_{\parallel} - \tilde{\ell}_{\parallel})^2 + \|\vec{\ell}_{\perp} - \tilde{\ell}_{\perp}\|_2^2, \quad (34)$$

$$\vec{x}^\top \mathbf{L}_G \vec{x} = \ell_{\parallel} \|\vec{x}\|_2, \quad \vec{x}^\top \mathbf{L}_{\tilde{G}} \vec{x} = \tilde{\ell}_{\parallel} \|\vec{x}\|_2. \quad (35)$$

Let $z = \tilde{\ell}_{\parallel} / \ell_{\parallel}$. Substituting (35) into (31), we see that \tilde{G} is a σ -spectral approximation of G if

$$\max \left\{ \frac{\tilde{\ell}_{\parallel}}{\ell_{\parallel}}, \frac{\ell_{\parallel}}{\tilde{\ell}_{\parallel}} \right\} = \max \left\{ z, \frac{1}{z} \right\} \leq \sigma. \quad (36)$$

Now, substituting (34) into (16), we obtain:

$$\begin{aligned} d_{\vec{x}}(\mathbf{L}_G, \mathbf{L}_{\tilde{G}}) &= \text{arccosh} \left(1 + \frac{((\ell_{\parallel} - \tilde{\ell}_{\parallel})^2 + \|\vec{\ell}_{\perp} - \tilde{\ell}_{\perp}\|_2^2) \|\vec{x}\|_2^2}{2\ell_{\parallel} \|\vec{x}\|_2 \tilde{\ell}_{\parallel} \|\vec{x}\|_2} \right) \\ &\geq \text{arccosh} \left(1 + \frac{\tilde{\ell}_{\parallel}^2 - 2\tilde{\ell}_{\parallel} \ell_{\parallel} + \ell_{\parallel}^2}{2\ell_{\parallel} \tilde{\ell}_{\parallel}} \right) \\ &\geq \text{arccosh} \left(\frac{1}{2} \left(z + \frac{1}{z} \right) \right). \end{aligned}$$

Using the identity $\text{arccosh}(x) = \ln(x + \sqrt{x^2 - 1})$,

$$\begin{aligned} d_{\vec{x}}(\mathbf{L}_G, \mathbf{L}_{\tilde{G}}) &\geq \ln \left(\frac{1}{2} \left(z + \frac{1}{z} \right) + \sqrt{\frac{1}{4} \left(z + \frac{1}{z} \right)^2 - 1} \right) \\ &\geq \ln \left(\frac{1}{2} \left(z + \frac{1}{z} \right) + \frac{1}{2} \left| z - \frac{1}{z} \right| \right) \\ &\geq |\ln(z)|. \end{aligned}$$

Thus, if $d_{\vec{x}}(\mathbf{L}_G, \mathbf{L}_{\tilde{G}}) \leq \ln(\sigma) \forall \vec{x} \perp \vec{1}$, then \tilde{G} is a σ -spectral approximation of G , as desired. \square

E Number of edges acted upon per iteration can be $\mathcal{O}(|V|)$

In this section, we study the effect of varying the parameter q , the fraction of sampled edges acted upon, using real-world datasets from different domains (Figure SI 4).

For each iteration of our algorithm, we sample a random independent edge set and act on the fraction q with the lowest β_{*e} (see Main Text Section 4). We find that the resulting error asymptotes around $q \sim 1/16$. We expect that by combining this sampling method with existing algorithmic primitives (eg, [20], see Appendix Section F), our algorithm could achieve a running time of $\tilde{\mathcal{O}}(\langle k \rangle |E|)$, where $\langle k \rangle$ is the average degree (see Main Text Section 4). This would allow it to be used in large-scale applications of graph reduction.

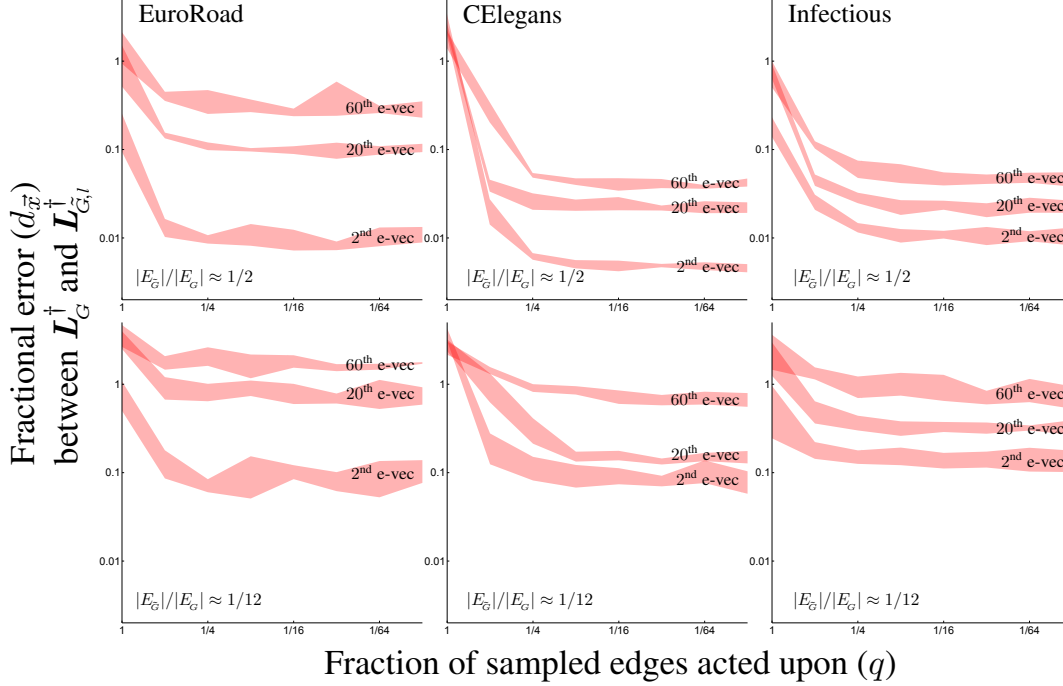


Figure SI 4: **Number of sampled edges acted upon per iteration can be $\mathcal{O}(|V|)$.** We study the effect of varying q , the fraction of the sampled edges that are acted upon per iteration, using three datasets: *Left*: a transportation network of European cities and roads between them (1039 nodes and 1305 edges) from [56]; *Middle*: the *C. elegans* posterior nervous system connectome (269 nodes and 2902 edges) from [52]; and *Right*: a weighted social network of face-to-face interactions during an exhibition on infectious diseases, with initial edge weights proportional to the number of interactions between pairs of people (410 nodes and 2765 edges) from [57]. We prioritize edge reduction (allowing for deletion, contraction, and reweighting). At each iteration, the algorithm randomly samples a maximal independent edge set, and chooses β such that a fraction q of these edges (with the lowest β_{*e}) are acted upon. For each run, we compute the hyperbolic distance $d_{\vec{x}}$ (fractional error) between $L_G^\dagger \vec{x}$ and $L_{G,l}^\dagger \vec{x}$, where \vec{x} is one of three eigenvectors of the original Laplacian. *Top* plots display the results when the graph has 1/2 of its original number of edges, and *bottom* plots when it has 1/12. Shading denotes one standard deviation about the mean for 8 runs of the algorithm for a given value of q . Note that a significant fraction ($q \sim 1/16$) of the sampled edges can be reduced each iteration without sacrificing much in terms of accuracy. As, empirically, the size of the independent edge sets are typically $\mathcal{O}(|V|)$, the number of edges acted upon per iteration can likewise be $\mathcal{O}(|V|)$.

F Efficiently computing m_e

As discussed in Main Text Section 4, the main computational bottleneck of our algorithm is computing Ω_e and m_e . For Ω_e , we can draw on the work of [20], which describes a method for efficiently computing ε -approximate values of Ω_e for all edges, requiring $\tilde{\mathcal{O}}(|E| \log |V| / \varepsilon^2)$ time. In this section, we describe an analogous procedure to efficiently compute the m_e .

Recall that the reduced Laplacian is:

$$\mathbf{L}_{\bar{G}} = \mathbf{W}_n^{-1} \mathbf{B}^\top \mathbf{W}_e \mathbf{B},$$

hence, the quantity $\widehat{\mathbf{L}}_{\bar{G}} \stackrel{\text{def}}{=} \mathbf{W}_n^{1/2} \mathbf{L}_{\bar{G}} \mathbf{W}_n^{-1/2}$ is clearly symmetric.

Less obvious is the fact that $\widehat{\mathbf{L}}_{\bar{G}}^\dagger \stackrel{\text{def}}{=} \mathbf{W}_n^{1/2} \mathbf{L}_{\bar{G}}^\dagger \mathbf{W}_n^{-1/2}$ is also symmetric. This can be seen by noting that $\mathbf{W}_n^{1/2} \mathbf{J} \mathbf{W}_n^{-1/2}$ is symmetric, and using the definition of the inverse (equation (26)):

$$\begin{aligned} \widehat{\mathbf{L}}_{\bar{G}}^\dagger &= \mathbf{W}_n^{1/2} \mathbf{L}_{\bar{G}}^\dagger \mathbf{W}_n^{-1/2} \\ &= \mathbf{W}_n^{1/2} \left((\mathbf{L}_{\bar{G}} + \mathbf{J})^{-1} - \mathbf{J} \right) \mathbf{W}_n^{-1/2} \\ &= \mathbf{W}_n^{1/2} (\mathbf{L}_{\bar{G}} + \mathbf{J})^{-1} \mathbf{W}_n^{-1/2} - \mathbf{W}_n^{1/2} \mathbf{J} \mathbf{W}_n^{-1/2} \\ &= \left(\mathbf{W}_n^{1/2} \mathbf{L}_{\bar{G}} \mathbf{W}_n^{-1/2} + \mathbf{W}_n^{1/2} \mathbf{J} \mathbf{W}_n^{-1/2} \right)^{-1} - \mathbf{W}_n^{1/2} \mathbf{J} \mathbf{W}_n^{-1/2}. \end{aligned}$$

We also remark that $\widehat{\mathbf{L}}_{\bar{G}}^\dagger$ is indeed the pseudoinverse of $\widehat{\mathbf{L}}_{\bar{G}}$:

$$\widehat{\mathbf{L}}_{\bar{G}}^\dagger \widehat{\mathbf{L}}_{\bar{G}} = \widehat{\mathbf{L}}_{\bar{G}} \widehat{\mathbf{L}}_{\bar{G}}^\dagger = \mathbf{I} - \mathbf{W}_n^{1/2} \mathbf{J} \mathbf{W}_n^{-1/2}$$

The change to the reduced Laplacian $\mathbf{L}_{\bar{G}}$ is given by

$$\Delta \mathbf{L}_{\bar{G}} = \mathbf{W}_n^{-1} \vec{b}_e \Delta w_e \vec{b}_e^\top$$

Thus, by the Woodbury matrix identity, the change to its inverse is

$$\Delta \mathbf{L}_{\bar{G}}^\dagger = f w_e \mathbf{L}_{\bar{G}}^\dagger \mathbf{W}_n^{-1} \vec{b}_e \vec{b}_e^\top \mathbf{L}_{\bar{G}}^\dagger$$

where f is given by equation (5).

Lifting this change back to the original dimension via equation (28) gives

$$\Delta \mathbf{L}_{G,i}^\dagger = f w_e \mathbf{C}^\top \mathbf{L}_{\bar{G}}^\dagger \mathbf{W}_n^{-1} \vec{b}_e \vec{b}_e^\top \mathbf{L}_{\bar{G}}^\dagger \mathbf{W}_n^{-1} \mathbf{C}$$

In particular, as $\mathbf{L}_{\bar{G}}^\dagger \mathbf{W}_n^{-1}$ is symmetric, $\Delta \mathbf{L}_{G,i}^\dagger$ is also symmetric, thus we can write the Frobenius norm as

$$\left\| \Delta \mathbf{L}_{G,i}^\dagger \right\|_F = f w_e \vec{b}_e^\top \mathbf{L}_{\bar{G}}^\dagger \mathbf{W}_n^{-1} \mathbf{C} \mathbf{C}^\top \mathbf{L}_{\bar{G}}^\dagger \mathbf{W}_n^{-1} \vec{b}_e \quad (37)$$

$$= f m_e \quad (38)$$

Note that the definition of m_e provided in Section 3.3 of the Main Text (equation (9)) applies to the case of unit node weights, and the general expression is given by

$$m_e = w_e \vec{b}_e^\top \mathbf{L}_{\bar{G}}^\dagger \mathbf{L}_{\bar{G}}^\dagger \mathbf{W}_n^{-1} \vec{b}_e, \quad (39)$$

where we have used $\mathbf{C} \mathbf{C}^\top = \mathbf{W}_n$.

Thus, we can express m_e in terms of $\widehat{\mathbf{L}}_{\bar{G}}^\dagger$:

$$\begin{aligned} m_e &= w_e \vec{b}_e^\top \mathbf{W}_n^{-1/2} \widehat{\mathbf{L}}_{\bar{G}}^\dagger \widehat{\mathbf{L}}_{\bar{G}}^\dagger \mathbf{W}_n^{-1/2} \vec{b}_e \\ &= w_e \left\| \widehat{\mathbf{L}}_{\bar{G}}^\dagger \mathbf{W}_n^{-1/2} \vec{b}_e \right\|_2^2. \end{aligned}$$

We can now use the Johnson–Lindenstrauss lemma to build a structure from which one can efficiently compute approximations of m_e . Let \mathbf{Q} be a random projection matrix of size $k \times n$, where $k = \mathcal{O}(\log n / \varepsilon^2)$, then one can compute ε -approximations of m_e as follows:

$$m_e \approx w_e \left\| \mathbf{Q} \widehat{\mathbf{L}}_{\bar{G}}^\dagger \mathbf{W}_n^{-1/2} \vec{b}_e \right\|_2^2.$$

Let $\mathbf{Z} = \mathbf{Q} \widehat{\mathbf{L}}_{\bar{G}}^\dagger$, and denote the i^{th} rows of \mathbf{Q} and \mathbf{Z} by \vec{q}_i and \vec{z}_i , respectively. Then, one can make k calls to an efficient algebraic multigrid solver (we used the *pyamg* package [58]) to obtain approximate solutions to $\widehat{\mathbf{L}}_{\bar{G}}^\dagger \vec{z}_i = \vec{q}_i$ for the k rows of \mathbf{Z} . An approximation to the m_e of any edge can now be computed by taking the difference between the columns of $\mathbf{Z} \mathbf{W}_n^{-1/2}$ corresponding to the two nodes jointed by this edge, and taking the squared 2-norm of the result.

F.1 Constructing the projection matrix

Care must be taken in constructing the projection matrix \mathbf{Q} . In particular, its rows must be orthogonal to the null space of $\widehat{\mathbf{L}}_{\widehat{G}}$, namely $\vec{w}_n^{1/2}$. In addition, the columns must be nearly unit length. To this end, we initialize \mathbf{Q} as a random matrix with entries $\{1/\sqrt{k}, -1/\sqrt{k}\}$ with equal probability and iterate the following steps:

1. For each column, scale its values such that it has unit length
2. For each row, subtract its weighted mean $\vec{q}_i^\top \vec{w}_n^{1/2} / \vec{1}^\top \vec{w}_n^{1/2}$

We iterate this procedure until the columns have nearly unit lengths, to within a factor sufficiently smaller than ε .

As a proof of concept, in Figure SI 5, we show the approximate m_e as a function of their exact values.

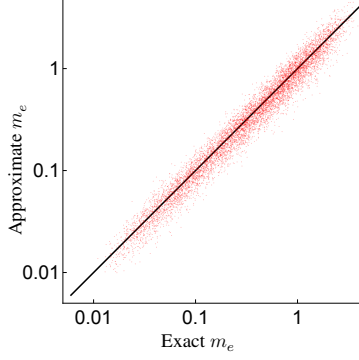


Figure SI 5: **Efficient approximation of m_e .** As a proof of concept, we compare the approximation of m_e (computed using the procedure described in this Section) with their exact values. Here, we consider a 64×64 torus graph (4096 nodes and 8192 edges), where the edge weights are randomly distributed as $\exp(U(-2, 2))$, where $U(a, b)$ is the uniform distribution. To calculate the approximate m_e , we project from 4096 to 33 dimensions, resulting in approximations that are typically within a factor of 1.27 of the exact value.

G Perturbations to eigenvalues of the Laplacian pseudoinverse

We first provide the lowest order change in the eigenvalues of \mathbf{L}_G^\dagger . Then, we show how it relates to the Frobenius norm of the perturbation, explicitly relating it to our graph reduction algorithm.

Consider an inverse Laplacian \mathbf{L}^\dagger , which has an eigenvector \vec{x} (without loss of generality, assume $\|\vec{x}\|_2 = 1$) with associated eigenvalue λ . If we perturb \mathbf{L}^\dagger by $\varepsilon \Delta \mathbf{L}^\dagger$, we can solve for the first-order corrections to this “eigenpair” as follows:

$$\begin{aligned} (\mathbf{L}^\dagger + \varepsilon \Delta \mathbf{L}^\dagger)(\vec{x} + \varepsilon \Delta \vec{x}) &= (\lambda + \varepsilon \Delta \lambda)(\vec{x} + \varepsilon \Delta \vec{x}) \\ (\mathbf{L}^\dagger - \lambda) \Delta \vec{x} &= (\Delta \lambda - \Delta \mathbf{L}^\dagger) \vec{x} + \mathcal{O}(\varepsilon), \end{aligned}$$

where we have used $\mathbf{L}^\dagger \vec{x} = \lambda \vec{x}$.

Taking the inner product with \vec{x} gives

$$\begin{aligned} \vec{x}^\top (\mathbf{L}^\dagger - \lambda) \Delta \vec{x} &= \vec{x}^\top (\Delta \lambda - \Delta \mathbf{L}^\dagger) \vec{x} \\ \Delta \vec{x}^\top (\mathbf{L}^\dagger - \lambda) \vec{x} &= \Delta \lambda \vec{x}^\top \vec{x} - \vec{x}^\top \Delta \mathbf{L}^\dagger \vec{x} \\ 0 &= \Delta \lambda - \vec{x}^\top \Delta \mathbf{L}^\dagger \vec{x}, \end{aligned}$$

where we have used the symmetry of \mathbf{L}^\dagger .

This provides the first-order correction to the eigenvalues of $\mathbf{L}^\dagger + \varepsilon \Delta \mathbf{L}^\dagger$:

$$\Delta \lambda = \vec{x}^\top \Delta \mathbf{L}^\dagger \vec{x}. \quad (40)$$

The correction in (40) is controlled by the operator norm of $\Delta \mathbf{L}^\dagger$,

$$\Delta \lambda = \vec{x}^\top \Delta \mathbf{L}^\dagger \vec{x} \leq \sup_{\|\vec{x}\|_2=1} \|\Delta \mathbf{L}^\dagger \vec{x}\|_2 = \|\Delta \mathbf{L}^\dagger\|_{\text{op}}.$$

Thus, bounding the first-order correction to the eigenvalues,

$$|\Delta\lambda| \leq \|\Delta\mathbf{L}^\dagger\|_{\text{op}}. \quad (41)$$

As the operator norm is bounded by the Frobenius norm (by the Cauchy–Schwarz inequality), the estimated error (ie, $\sum \mathbb{E} \|\Delta\mathbf{L}^\dagger\|_{\text{F}}^2$, equation (18)) provides a conservative bound for the change in the eigenvalues of the resulting reduced graph.

Moreover, as the bound is the same for all eigenvalues of the perturbed \mathbf{L}^\dagger , the *relative* error is more tightly bounded for its largest eigenvalues (those associated with large-scale structure).

H Comparison of graph reduction methods using typical similarity measures

Our proposed hyperbolic distance is not usually used as a measure of similarity. Hence, in this section, we show that other more commonly used measures yield similar results when comparing graph reduction algorithms.

H.1 Sparsification

Figure SI 6 compares our algorithm (prioritizing edge reduction, and excluding the possibility of contraction) with the spectral sparsification algorithm of [20] using a stochastic block model (SBM) with four distinct communities. We choose a highly associative SBM due to the clear separation between the eigenvectors associated with global structure (ie, the communities) and the bulk of the spectrum. Note that these algorithms have different objectives (preserving \mathbf{L}^\dagger and \mathbf{L} , respectively), and both accomplish their desired goal.

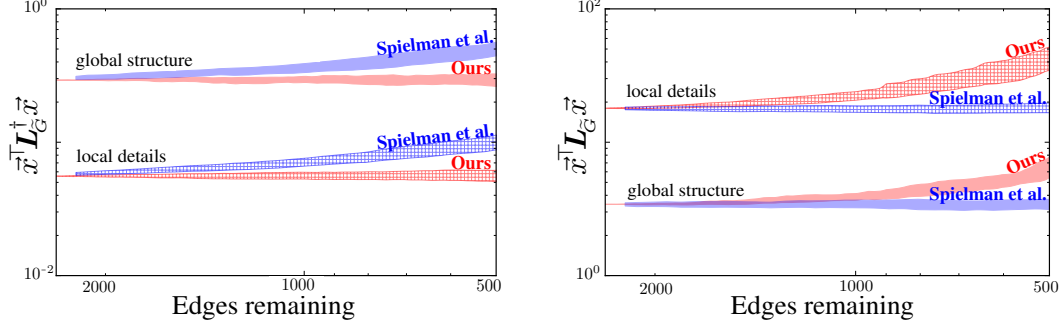


Figure SI 6: **Our sparsification algorithm preferentially preserves global structure.** We compare our algorithm without contraction (in red) with that of Spielman & Srivastava [20] (in blue) using a symmetric stochastic block model (256 nodes, 4 communities, and intra- and inter-community connection probabilities of 2^{-2} and 2^{-6} , respectively). We ran both algorithms 16 times on the same initial graph. For each eigenvector of the original Laplacian, we compute the mean and standard deviation of its quadratic forms (with \mathbf{L}_G^\dagger and with \mathbf{L}_G) as a function of edges remaining. We divide the eigenvectors into two groups: the 3 nontrivial eigenvectors (“global structure”) and the remaining eigenvectors (“local details”), and compute the average mean and average standard deviation for each group. Shading denotes one (average) standard deviation about the (average) mean. *Left:* Laplacian pseudoinverse quadratic form. *Right:* Standard Laplacian quadratic form. Note that the upward bias of the “reciprocal” quadratic form is expected for both algorithms (as $\mathbb{E}[X] \leq 1/\mathbb{E}[1/X]$ for any random variable $X > 0$).

H.2 Coarsening

Figure SI 7 replicates the results of Figure 3, but uses the Laplacian pseudoinverse quadratic form to measure the reduction quality instead of our proposed hyperbolic distance.

Figure SI 8 compares our method with that of Loukas [55], using the average relative error of the k lowest non-trivial eigenvalues of the Laplacian (ie, $\frac{1}{k} \sum_{i=2}^{k+1} |\tilde{\lambda}_i - \lambda_i|/\lambda_i$) to measure the reduction quality.

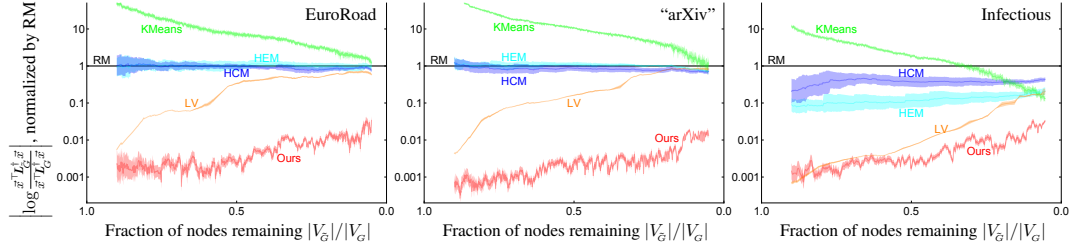


Figure SI 7: **Our coarsening algorithm performs even better when using the quadratic form with L^{\dagger} .** Here we replicate the experiments in Figure 3. However, instead of using our proposed hyperbolic distance, we consider the logarithm of the fractional change in the Laplacian pseudoinverse quadratic form for \vec{x} the lowest non-trivial eigenvector of the original Laplacian: $|\log(\vec{x}^T L_G^{-1} \vec{x} / \vec{x}^T L_G^{\dagger} \vec{x})|$. As before, for each algorithm, we plot the mean of this quantity normalized by that obtained by random matching (RM). Shading denotes one standard deviation about the mean for 16 runs of the algorithms. The results are remarkably similar to those obtained using our proposed hyperbolic distance (Figure 3). The most notable deviation is that our algorithm appears to perform *better* when compared using this quadratic form.

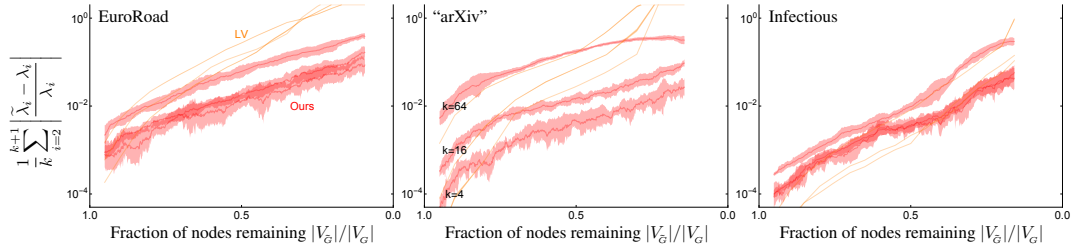


Figure SI 8: **Our algorithm preferentially preserves the lower portion of the Laplacian spectrum.** We compare our coarsening algorithm (**Ours**) with that of Loukas [55] (**LV**) using the same three datasets as in Figure 3. We use the relative error in the k lowest non-trivial eigenvalues of the Laplacian: $\frac{1}{k} \sum_{i=2}^{k+1} |\tilde{\lambda}_i - \lambda_i| / \lambda_i$, a measure of spectral similarity considered in [55]. Shading denotes one standard deviation about the mean for 8 runs of the algorithms. Note that our algorithm performs considerably better when applied to graphs with a geometric quality.

I Applications to graph visualization

Data visualization is an important (and aesthetically pleasing) application of graph reduction. As such, we generated videos of our algorithm reducing several real-world datasets. Figure SI 9 displays several stages of our algorithm applied to a temporal social network. A video of this reduction can be found [here](#); an application to an airport network (a case with both geometric and scale-free aspects) can be found [here](#); an application to the European road network can be found [here](#), and a reduction of a “hierarchical meta-graph” can be found [here](#).¹

¹Explicit urls for the non-hyperlinked:

[youtube.com/watch?v=qqLJc1VUML8](https://www.youtube.com/watch?v=qqLJc1VUML8); [youtube.com/watch?v=tXUr6BRaEI](https://www.youtube.com/watch?v=tXUr6BRaEI);
[youtube.com/watch?v=UVhT0y4Uae0](https://www.youtube.com/watch?v=UVhT0y4Uae0); and [youtube.com/watch?v=i3u4kkxMK40](https://www.youtube.com/watch?v=i3u4kkxMK40).

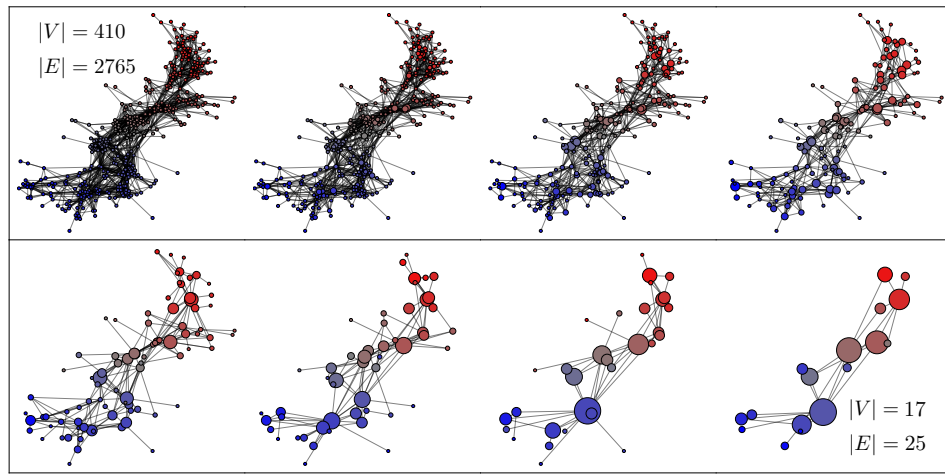


Figure SI 9: **Visualization of our graph reduction algorithm preserving global structure.** We applied our algorithm (prioritizing edge reduction, and allowing for deletion, contraction, and reweighting) to a weighted social network of face-to-face interactions during an exhibition on infectious diseases, with initial edge weights proportional to the number of interactions between pairs of people (410 nodes and 2765 edges) from [57]. Node color indicates the lowest nontrivial eigenvector of the reduced Laplacian, which in this case is aligned with the temporal direction. This graph displays a notable amount of hierarchical clustering (owing to its social nature), which is reflected in the reduced graphs. Eg, our algorithm begins by collapsing small, tightly-knit clusters of several people into one “supernode”, corresponding to groups of people who visited the exhibition together. A video of this reduction can be found [here](#).